On the Uncertainty Quantification of Roll Decay Test

Shawn Aram, *David Taylor Model Basin (NSWCCD),* shawn.aram.civ@us.navy.mil
Joel T. Park, *David Taylor Model Basin (NSWCCD),* joel.t.park.civ@us.navy.mil

ABSTRACT

This paper focuses on methods of processing ship roll decay data. Analysis is performed on Computational Fluid Dynamics (CFD) results for the Office of Naval Researh Tumblehome (ONRTH) configuration. CFD prediction is compared to experimental measurments of a 1/49 scale model at 9.3° roll amplitude. Traditional log decrement method is revisted from a more formal point of view of multi-dimensional linear regression. Calculation of confidence and prediction intervals are caried out for uncertainty assessment. As ONRTH configurion is known for its geometic nonlinearity, outlier analysis with Cook's distances and thier influence on uncertainty is described. The paper also describes a nonlinear regression with a decaying cosine function that is fitted to the data and its uncertainty is evaluated. Splitting data in two subsets is considered as a way to account for geometric nonlinearity.

Keywords: *Roll decay, Uncertainty Quantification*

1. INTRODUCTION

A roll decay test remains a popular way to estimate roll damping, e.g. ITTC (2021) recommended procedure 7.5.-02-07-04.5. Large uncertainty in experimental data is an indication of complex physics of roll damping as also described for three hull forms in Park *et al.* (2009). One of the major contributors to this uncertainty is the data processing.

Calculation of ship motions (both in frequency- and time-domain) is a main consumer of roll damping data. Accuracy of the roll motion calculation near synchronos or parametric resonance conditions may be signficantly affected by the uncertainty of roll damping. Propagating the roll damping uncertainity through dynamical system may lead to more relaible evaluation of ship motions.

The principal idea of uncertainty propagation seems to be straight forward. The roll damping coefficients are considered as random variables. Their statistical properties should be found from the uncertainty analysis. Then the dynamical system can be considered as a deterministic function of random variables, leading to a distribution of the responce.

Recently some studies were carried out for reduced-order modeling (ROM) of ship motions within the multi-fidelity framework (e.g. Pipras, *et al.* 2022, Levine *et al.* 2022). It became clear that uncertainty quantification of reduced order models is essential for gaining confidene in application of the multi-fidelity framework (see also a review by Weems and Sapsis 2022 to be presented at this workship). Uncertainty is seen as ”price” one pays for using ROM instead of high-fidelity mathematical model.

Essentially, polynomial representation of roll damping is a ROM. Choice of using a quardatic, quadratic plus cubic or an equivalent linear damping model depends on a problem in hand. For example, if the objective is an estimation of standard deviation of roll motions with time-domian simulation, the nonlinearity of roll damping may not be essential (as it may be averaged out). Then, one could prefer a model with minimum uncertainty. When the objective is large roll angle excursion or capsizing simulation, the choise may be different.

Different damping models and different fitting techniques may differ in uncertainty. *E.g.* application of the curve fitting technique (Park *et al.* 2016 and 2017) demonstrates less uncertainty, compared to traditional log decrement method, but produces only a linearized roll damping coefficient.

This paper revisits the curve fitting technique (Park *et al.* 2009, 2016, and 2017) as well as the traditional logarithmic decrement approach. The focus of this study, however, is not a comparison, but a review of assumptions and an attempt for a more formal uncertainty analysis of roll decay data.

Many factors exist in a physical roll decay experiment that cannot be explicitly identified and cannot include the uncertainty, such as the influence of wave reflection or the manual initiation of roll decay. For consistant data analysis uncertainty, roll decay results of numerical simulations are considered.

ONR tumblehome topside configuration (Bishop *et al.* 2005) is considered as a ship model for the current study. This configuration which is known for its geometric nonlinearity and reflected in the dependence of natural roll frequency to amplitude, offers a proper “stress test” to standard assumptions of roll decay analysis.

2. CFD ANALYSIS OF ROLL DECAY

Numerical Methodology

Star-CCM+, which is a commercial CFD simulation software developed by Siemens Digital Software, is employed to perform roll decay modeling. Navier-Stokes equations in the software are solved with finite-volume method, where surface and volume integrals representing convective and diffusive fluxes are approximated with the mid-point rule. The segregated solution of the velocity-pressure coupling problem is obtained with a Semi-Implicit Method for Pressure Linked Equations (SIMPLE) algorithm. An implicit second-order three-level scheme is adopted for time integration. The free-surface is modeled by the Volume of Fluid (VOF) method with a High- Resolution Interface Capturing (HRIC) scheme for tracking the sharp interface between water and air. Anisotropic refinement allows building efficient grids for the HRIC scheme.

Ship motions in Star-CCM+ can be modeled with the overset grid method, which allows multiple

grids within one computational background domain to overlap arbitrarily. Rigid body motions are handled by the Dynamic Fluid Body Interaction (DFBI) method. Both 6 degrees of freedom (6DoF) motions and motions with constrained modes can be modeled.

CFD Setup

Figure 1 is the ONRTH model geometry for this study. It is a fully appended 1/49 scale model, Model 5613, equipped with a skeg, bilge keels, twin rudders, shafts and two 4-bladed propellers mounted with shaft brackets. Except the twin propellers, all appendages are considered in this analysis. Table 1 gives the model particulars extracted from the SIMMAN2020 Workshop websitesite on Verification and Validation of Ship Maneuvering Simulation Methods, http://www.simman2019.kr.

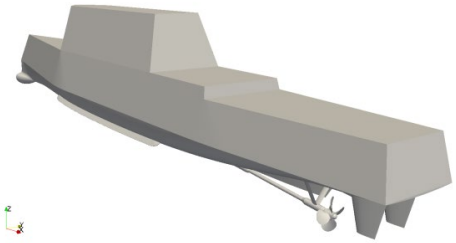

Figure 1: ONRTH model.

Table 1: Particulars for model scale ONRTH.

Main Particulars	Model Scale
Displacement, Δ (kg)	72.6
Waterline Length, L (m)	3.147
Waterline Beam, B (m)	0.384
Draft, T (m)	0.112
Wetted Surface Area, S (m^2)	1.5
LCB (m aft of FP)	1.625
VCG (m from keel)	0.156
Roll Radius of Gyration, k_{xx}/B	0.344
Pitch Radius of Gyration, k_{yy}/L	0.246
Yaw Radius of Gyration, k_{zz}/L	0.246
Propeller Diameter, D_p (m)	0.1066
Propeller Shaft Angle (deg)	5

Unsteady Reynolds-Averaged Navier-Stokes (URANS) simulation of the roll decay is performed in Star-CCM+, with two equation SST k-ω model as the turbulence model. Figure 2 is a view of computational grid generated for this simulation in calm water condition. Hexahedral-dominant unstructured-grid topology with prism layers for boundary layer is employed to discretize the computational domain. Two regions including background and ship are created, with ship defined as overset region to allow relative motions of the ship with respect to the background region. Two grid resolutions with 5.7×10^6 (Grid1) and 23.7×10^6 (Grid2) cells are applied for a limited grid sensitivity analysis, where the base size of Grid2 cell is 0.125 of Grid1 (0.5 in each principal direction).

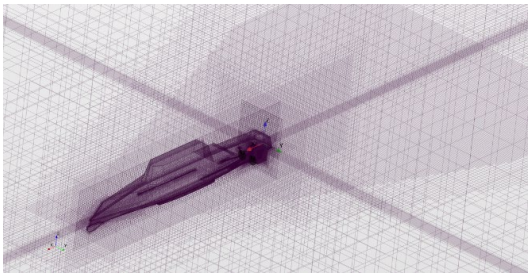

Figure 2: Computational grid for calm water roll decay simulation in Star-CCM+.

CFD Validation

The CFD results of the roll decay simulation is validated against the experimental data collected at the University of Iowa Wave Basin Facility, IIHR. This data set is labeled EFD in this paper. The origin of the ship-fixed coordinate system defined in Star-CCM+ is at the center of gravity with x+ towards bow, y+ towards port, and z+ up.

The CFD prediction of roll decay is performed for Froude number, Fr = 0. The model is free in 6DoF and released with an initial roll angle of 9.3°, which matches the model test. Figure 3 compares the time history of predicted and measured roll motion, φ. Grid1 resolution is selected for this comparison. A reasonable agreement is obtained between the CFD and model test.

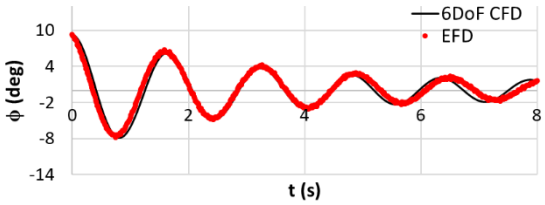

Figure 3: Time history of roll angle at *Fr* = 0.

The predicted roll motion is further evaluated by calculating the roll decay coefficient (η_j) and peak period (T_j) defined as follows:

$$\eta_j = \frac{1}{\pi} ln\left(\frac{a_j}{a_{j+1}}\right), \epsilon_j = \frac{1}{2}\left(a_j + a_{j+1}\right) \qquad (1)$$

$$T_j = t_{j+2} - t_j \quad (2)$$

where, a_j is the absolute peak roll angle at time t_j, and index j is an integer number that represents the sequence of roll peaks. These two parameters are plotted in Figure 4 for both CFD and experiment. Except the small roll angles ($\epsilon_j < 2$), both the roll decay coefficient and peak period are accurately predicted by 6DoF CFD. The non-linear trends seen in EFD for both parameters at $\epsilon_j < 2$ are likely related to the uncertainty in the measurement for low amplitude roll motions, waves in the basin produced by the roll initiation, and electronic noise in the roll instrumentation.

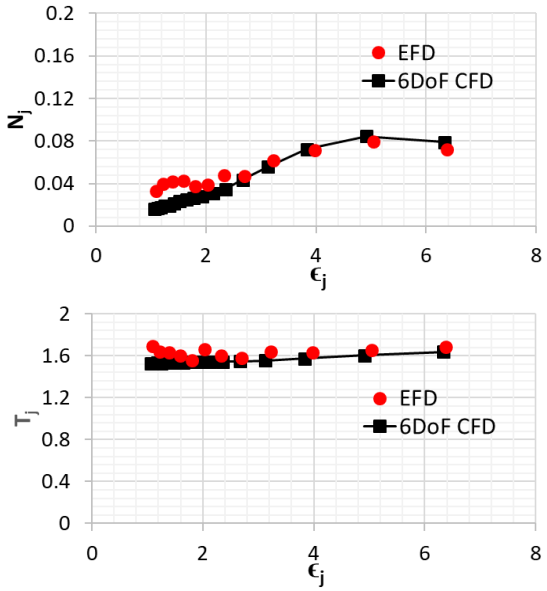

Figure 4: Roll decay coefficient and peak period at *Fr* = 0.

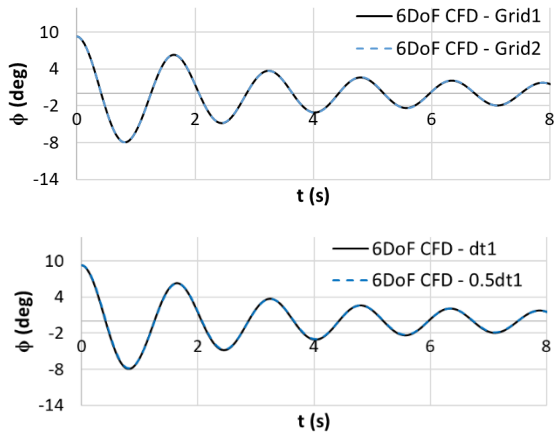

Figure 5: Sensitivity analysis of roll decay prediction to the spatial and temporal resolutions.

The sensitivity of the roll decay prediction to the spatial and temporal resolutions is depicted in Figure 5, where an independence of computed roll motion to the grid spacing and time step size is observed. The analysis is performed for the CFD predicted roll decay with initial roll angles of 6°, 9.3° and 12°.

3. LOG-DECREMENT METHOD

Background and Assumptions

The logarithmic decrement method is one of the basic technique adopted by the ship hydrodynamic community for modeling the roll damping. The data are presented as

$$\varphi_i = \frac{1}{2}(a_i + a_{i+1}) \quad (3)$$

$$LD_i = \frac{a_i - a_{i+1}}{\pi \varphi_i} \quad (4)$$

where a_i are "amplitudes", i.e. absolute values of peaks and LD is a logarithmic decrement, reflecting an energy lost with each semi-period of oscillation.

Being a classical one, the log-decrement method has originated from the solution of homogenous linear differential equation from Lloyd (1998) and Myklestad (1956):

$$\varphi(t) = a\exp(-\delta t)\cos(\omega_1 t + \theta) \quad (5)$$

where amplitude a and phase θ are arbitrary constants, depending on initial conditions, ω_1 is a frequency of free damped oscillation, and δ is a dimensional damping coefficient. If the linear case is completely applicable, the LD-value will be constant.

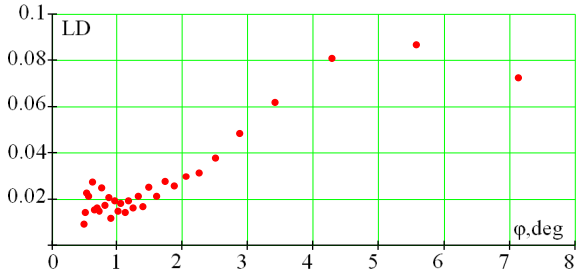

Figure 6: Roll decrement versus amplitude.

From Figure 6, the data do not show a constant behavior, due to a well-known fact that the roll damping depends on the roll amplitude. The decay coefficient by the log-decrement method is plotted as a function of the average absolute values of two sequential peaks in the time series. The peaks are a function of time; consequently, the data are plotted as reverse time. That is, the small peaks occur later in time, while the larger peaks exist earlier in time. Common practice recommended in SDC 8/WP.4/Add.2 is to approximate roll decay data with a quadratic polynomial

$$F(\varphi) = c_0 + c_1\varphi + c_2\varphi^2 \quad (6)$$

where c_0, c_1 and c_2 are the decay extinction coefficients.

For the time domain simulations, the dependence of roll damping on roll amplitude is modelled as a cubic function of roll rate:

$$f_d(\dot{\varphi}) = 2\delta\dot{\varphi} + \beta|\dot{\varphi}|\dot{\varphi} + \gamma\dot{\varphi}^3 \quad (7)$$

where $\dot{\varphi}$ is roll rate and (Bulian 2004) and

$$\delta = 2c_0\omega_1 \quad (8)$$

$$\beta = \frac{3\pi}{4}c_1 \quad (9)$$

$$\gamma = \frac{8}{3\omega_1}c_2 \quad (10)$$

These coefficients are found with a multi-dimensional linear regression.

Linear Regression

The logarithmic decrement (in a vector form) is presented as

$$\overrightarrow{LD} = \vec{y} = \mathbf{X}\cdot\hat{\vec{c}} + \vec{\varepsilon} \quad (11)$$

where $\vec{y}$ is usually referred as response vector or vector of dependence variables, $\hat{\vec{c}}$ is a vecor of parameters, the "hat" $\hat{}$ symbol indicates that the value is an estimate being a random number, and $\mathbf{X}$ is a matrix of predictors defined as

$$X_{i1} = 1, X_{i2} = \varphi_i,\ X_{i2} = (\varphi_i)^2,\quad y_i = LD_i \quad (12)$$

The vector $\vec{\varepsilon}$ is called a vector of disturbance terms, error variables, or residuals and is defined as a difference between a vector of predicted variables $\vec{y}$ and predicted values $\hat{\vec{y}}$, ($\vec{\varepsilon} = \vec{y} - \hat{\vec{y}}$).

This regression is referred as linear since the relationship between a scalar response (dependent variable) and vector of regressors (independent variables, predictors) is linear. The regression equation for a given data set can be presented in the following form:

$$\hat{\vec{y}} = \mathbf{X}\cdot\hat{\vec{c}} \quad (13)$$

The estimates of vector $\hat{\vec{c}}$ is caluclated as:

$$\hat{\vec{c}} = \left(\mathbf{X^T X}\right)^{-1}\mathbf{X^T}\vec{y} \quad (14)$$

The elements of the parameter vector are interpreted as the partial derivatives of the dependent variable with respect to the various independent variables, in which the matrix expression $\left(\mathbf{X^T X}\right)^{-1}\mathbf{X^T}$ is a result of the mean square fit (i.e. differentiating the residuals by the coefficients and setting them to zero in order to minimize the error terms). From the vector of residuals, a standard residual error is estimates as:

$$\hat{\sigma}^2 = \frac{1}{n-p}\vec{\varepsilon}\vec{\varepsilon}^T \quad (15)$$

where n is the number of dependent variables and p is the number of predictors.

In addition to standard residual error, the coefficient of determination of variance explained, R^2 can evaluate a model. This coefficient varies between 0 to 1, where 1 means 100 % fit of model to the data set, and is defined as follows:

$$R^2 = \frac{(\hat{\vec{y}}-\hat{m}_y)^T\cdot(\hat{\vec{y}}-\hat{m}_y)}{(\vec{y}-\hat{m}_y)^T\cdot(\vec{y}-\hat{m}_y)} \quad (16)$$

where $\hat{m}_y$ is a mean value estimate of $\vec{y}$.

Uncertainty Quantification of Linear Regression

The main underlying probabilistic assumption of regression is normal distribution of residuals. This assumption is that the regression model fits data well and deviations are caused by a large number of reasons, so normality of residuals follows from the central limit theorem.

Like any other statistical estimates, the estimates of parameters $\hat{\vec{c}}$ are random quantities. As they are result of averaging, they have Student's t-distribution like any other average of normal variable (which are the residuals in this case). The uncertainty of i-th parameter is characterized with a confidence interval with the following boundaries:

$$\hat{c}_i^{up,low} = \hat{c}_i \pm t_{n-p}^{\alpha/2}\hat{\sigma}\sqrt{(\mathbf{X^T X})^{-1}_{ii}} \quad (17)$$

where α is a complimentary to a given confidence probability (i.e. 0.05 for the confidence probability of 0.95) and $t_{n-p}^{\alpha/2}$ is the $\alpha/2$ quantile of Student's t-distribution. For the large number of points (25 and more), Student's t-distribution is not really distinguishable from normal and assumption of normality of residuals can be relaxed due to the Central Limit Theorem.

As the parameters of $\hat{\vec{c}}$ are random numbers, the predicted values $\hat{\vec{y}}$ are also random numbers since they have resulted from the regression Equation (11), which is a deterministic function of random arguments. Thus, its statistical uncertainty (i.e. caused by the finite volume of data) should be quantified with the known distribution of the

parameters of the $\hat{\vec{c}}$ vector. Since the regression Equation (11) is linear, the predicted values also follow the Student's *t*-distribution and the boundaries of confidence interval are expressed as:

$$\hat{y}_i^{u,l} = \hat{y}_i \pm t_{n-p}^{\alpha/2}\hat{\sigma}\sqrt{\vec{x}_i^T(\mathbf{X}^\mathbf{T}\mathbf{X})^{-1}\vec{x}_i} \qquad (18)$$

where $\vec{x}_i$ is the *i*-th row of matrix **X**.

The other type of uncertainty, associated with regression, is the prediction uncertainty, quantified with the prediction interval:

$$\hat{y}_i^{u1,l1} = \hat{y}_i \pm t_{n-p}^{\alpha/2}\hat{\sigma}\sqrt{1+\vec{x}_i^T(\mathbf{X}^\mathbf{T}\mathbf{X})^{-1}\vec{x}_i} \qquad (19)$$

As its name suggests, the prediction interval quantifies uncertainty of prediction, i.e. applying the regression formula to estimate a "new" value of *y*. Its interpretation in terms of propagation of roll decay uncertainty though a dynamical system is not clear at the moment. Further study includes both statistical and prediction uncertainty.

Geometrical Nonlinearity

As already mentioned, the ONRTH hull is known for its geometric nonlinearity due to its topside configuration. This nonlinearity is reflected in a shape of its backbone curve in Figure 7. While for a more conventional hull form, deviation of the backbone curve from the vertical line is expected to be significant around 10 degrees, Figure 7 demonstrates practically no vertical portion of the backbone curve for the ONRTH, as its waterplane changes significantly even for small roll angles.

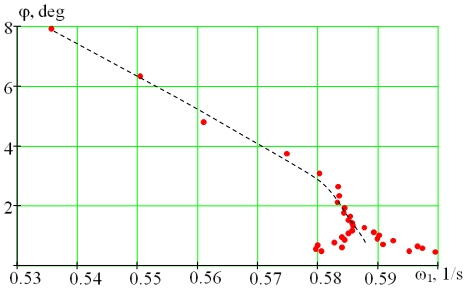

Figure 7: Backbone curve.

Traditional technique for the roll decay test includes implicit assumption for the independence of amplitude and period. This could be a reason for excluding the first peak in the record. Choosing the initial condition slightly above the independence range may be helpful to obtain a "cleaner" record as the initial disturbance may dissipate when the model enters the range of independence.

Analysis of Influential Values

The range of indolence between amplitude and period does not exist for the ONRTH. At the same time CFD simulation may not have those "initial disturbances" that may present in a physical experiment. The large peaks may have a large influence on regression results.

In order to estimate the influence of a data point in a regression analysis, Cook's distance (Cook's D) is employed, in which the a fitted model without a selected data point (*i*) is compared with a model based on all data points. As a result, a total of *n* checks will be made. The Cook' D of i-th dependent variable can be calculated with:

$$D_i = \frac{(\varepsilon_i)^2}{p\sigma_r^2}\frac{h_{ii}}{(1-h_{ii})^2} \qquad (20)$$

where h_{ii} is the i-th diagonal element of project (influence) matrix $\boldsymbol{H}$. This matrix maps the vector of dependent variables ($\vec{y}$) to the vector of fitted values ($\hat{\vec{y}}$), and identifies the influence of each response value on each fitted value. Similarly, the diagonal elements of the projection matrix called leverages describe the influence of each response value on the fitted value for that same observation. The project matric can be obtained from:

$$\boldsymbol{H} = \boldsymbol{X}\left(\boldsymbol{X}^\boldsymbol{T}\boldsymbol{X}\right)^{-1}\boldsymbol{X}^\boldsymbol{T} \qquad (21)$$

Data points with large residuals (outliers) or high leverage could distort a fitted model. Cook's Distance, which essentially measures the effect of deleting a data point is evaluated in the current study to exclude the outliers from the model. The Cook Distance D_i is considered large if it is greater than three times of the mean value of elements of vector $\vec{D}$ ($D_i > 3\mathbb{E}(\vec{D})$).

From the time history of roll angle with 32 roll peaks as independet variables, the degrees of freedom for this time series becomes 29 (32 (variables) – 3 (parameters)). The elements of parameter vector $\hat{\vec{c}}$ obtained from Equation (14) are summeried in Table 2 for the three roll decay simulations. A large variation of these elements with respect to the initial roll angle is observed, which could be an indication for dependency of roll damping coefficient to this parameter.

Table 2 Elements of $\hat{\vec{c}}$.

a (deg)	c_0 ($\times 10^3$)	c_1 ($\times 10^3$)	c_2 ($\times 10^3$)
6	4.32	1.4	-0.20
9.3	2.78	1.8	-0.92
12	-0.85	2.1	-1.18

From the elements of vector $\hat{\vec{c}}$, the fitted model is constructed. The boundaries of confidence and prediction intervals of the parameter vector are calculated next and fitted model and boundaries are plotted against data in Figure 8. The model for the 6° initial angle is close to a linear trend, while it is non-linear for the higher initial angles. The prediction interval is fairly wide and the intercept of the lower boundary is negative for all three cases, which is not physcial. To quantfy the uncertainty of the model, $\hat{\sigma}^2$ and R^2 are also calculated and summerized in Table 3. The residual error for three case is comparable between three cases, but R^2 increases as the initial roll angle goes up, which is an indication for a closer fit of the model to the data.

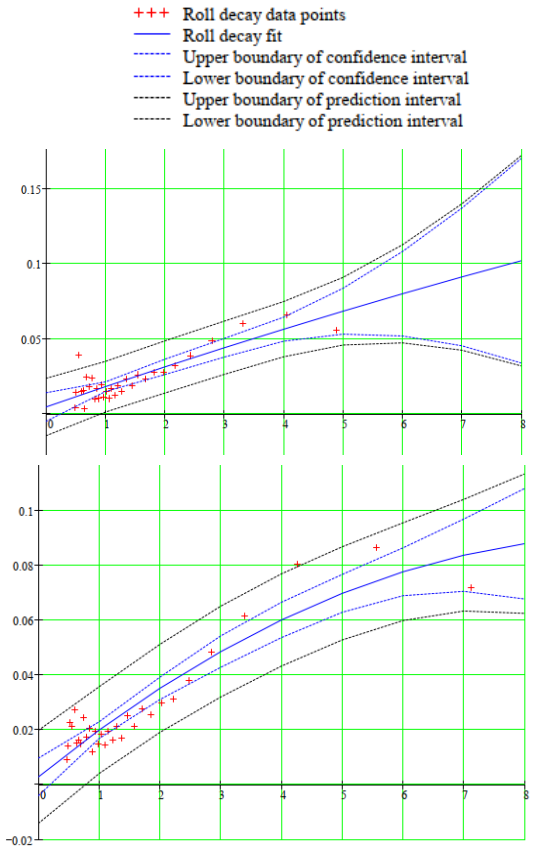

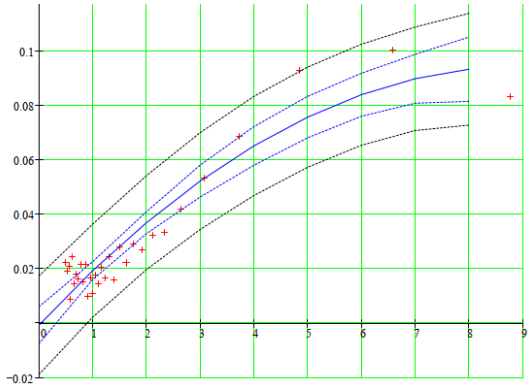

Figure 8: Fitted model, conficence interval and prediction interal of logarithmic decrenet with initial roll angle of 6° (top), 9.3° (middle) and 12° (bottom).

Table 3 Standard residual error and R^2 of the fitted model

a (deg)	$\hat{\sigma}^2$	R^2
6	8.118E-03	0.75
9.3	7.611E-03	0.865
12	8.221E-04	0.89

Cook's Distance method identifies potential outliers and improve the fitted model. This process is performed three times and for every set of points that are removed, the model is refitted to the new dataset and confidence and prediction intervals are recalculated. Figure 9 depicts the refitted model and coresponding intervals for the first (top row), second (middle row) and third (bottom) outlier removal and initial roll angle of 9.3°. One point per step is identified as an outlier. The intercept of lower prediction interval turns to a positive value after removing the second outlier and the refitted model tends to matches closer to the data points. The slope of the model approaches to zero through this process. R^2 of the fitted model is calculated at each step to determine the cut off point for the outlier removal process. Table 4 summerizes the R^2 value of the refitted model for all three initial angles, which increases compared to the original model for the first and second steps, but it does not noticably impove for the third step. This implies that the R^2 could be a criterion for identifying the number of steps required to improve a model.

Table 4: variance of fitted model.

	a (deg)		
R^2	6	9.3	12
Original data	0.75	0.86	0.89
First point-removal	0.78	0.91	0.92
Second point removal	0.86	0.93	0.94

Third point removal	0.77	0.87	0.89

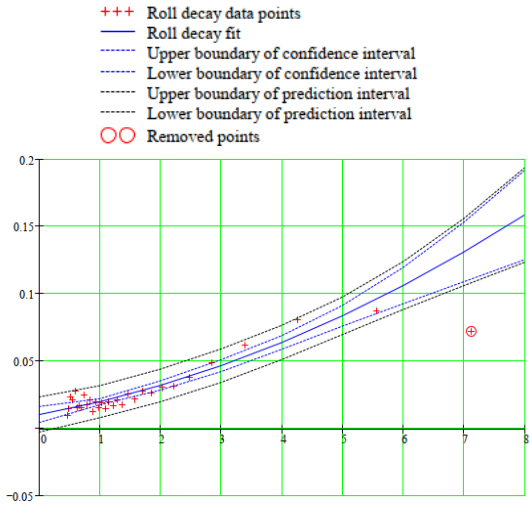

(a) First point-removal

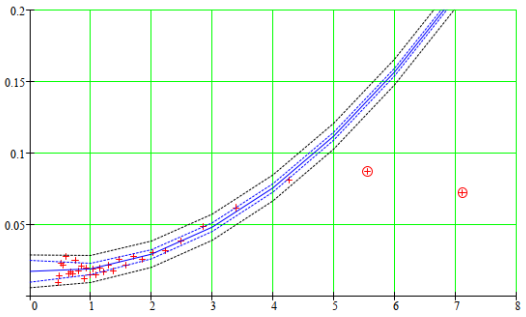

(b) Second point-removal

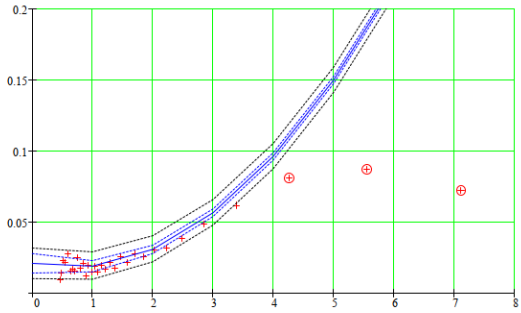

(c) Third point-removal

Figure 9: Cook's Distance method for roll decay data with initial roll angle of 9.3°.

Table 5 compares the elements of vector $\hat{\vec{c}}$ resulting from the original data set and the second point-removal step. Significant difference between the parameters of two data sets is observed. A strong dependency of the model coefficients to the initial roll angle is also seen for the refitted model, which is consistent with the original model.

Table 5: Elements of vector $\hat{\vec{c}}$ calculated from the original data points and the second point-removal step.

	a (deg)	c_0 (×10³)	c_1 (×10³)	c_2 (×10³)
Original data set	6	4.32	1.4	-0.2
	9.3	2.78	1.8	-0.92
	12	-0.84	2.1	-1.18
Second point-	6	1.1	-0.44	4.69
	9.3	1.7	-2.65	4.31
	12	1.4	0.91	3.34

4. EXPONENTIAL COSINE FUNCTION

For experimental data, the data may be fitted directly with Equation (5). A more general form appropriate for experimental data that includes offset is given by the following equation

$$\varphi = aexp(-bt)\cos(2\pi t/c + d) + e \qquad (22)$$

where a is the amplitude, d the phase shift, and e the offset. The period T and the decay coefficient η are defined as

$$T = c \qquad (23)$$

$$\eta = bc/(2\pi) \qquad (24)$$

Single Data Set

The curve fit of the time series for the CFD and experimental results at 9.3°amplitdes is indicated in Figure 10 and 11. The duration of each run is 26 s. The results are presented as time series of roll angle and and residual (difference between the curve fit and the data). The offset, e, is non-zero for both the CFD and experimental results. The 95 % prediction limit for the experimental data is about half that of the CFD. The data trends are similar. That is, the curve fit under predicts the measured roll amplitude of 9.3°. The manual initiation of the roll amplitude may be the cause in the difference between the predicted and measured roll amplitude. A similar result was observed in Park *et al*. (2009).

Split Data Set

The deviation from the curve fit at the smaller roll angles is evident in the plots of Figure 10 and 11. Similar trends are observed for the two other initial roll angles in CFD (not shown here). The curve fit of the time series is improved by splitting the series in two parts at the nearest peak after 6 s. The results are in Figure 12 through Figure 15 for amplitudes of 6° through 12°, respectively. In all cases, the curve-fitted amplitude in the first 6 s is nearer the actual intitial CFD amplitude and the measured amplitude for 9.3°. The best curve-fit is at 6 s with a curve fit amplitue of 9.316° ±0.081° (±0.87 %) or a difference

of 0.17 % from the measured amplitude of 9.3°. The difference is smaller than the uncertainty estimate. The amplitude comparison is summarized in Table 6.

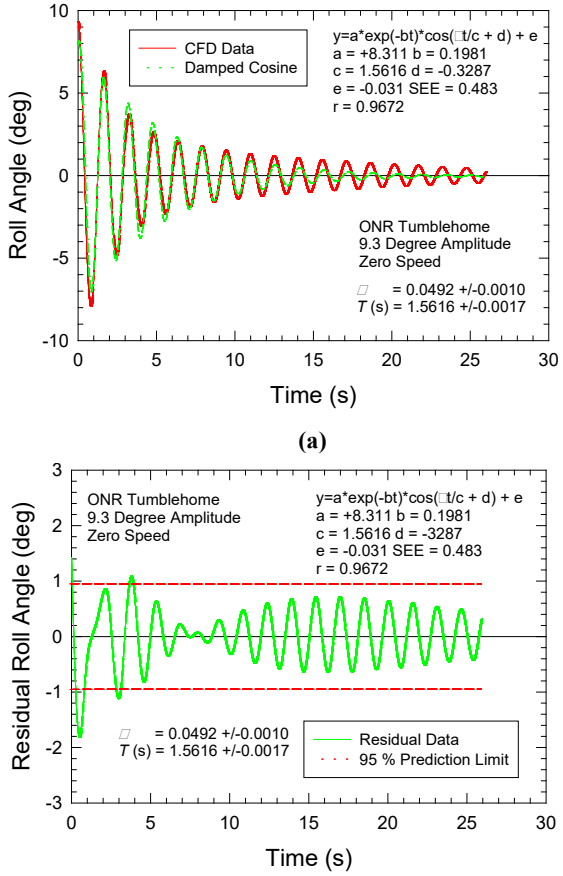

Figure 10: Time series of (a) roll angle and (b) residual at 9.3° with all CFD data.

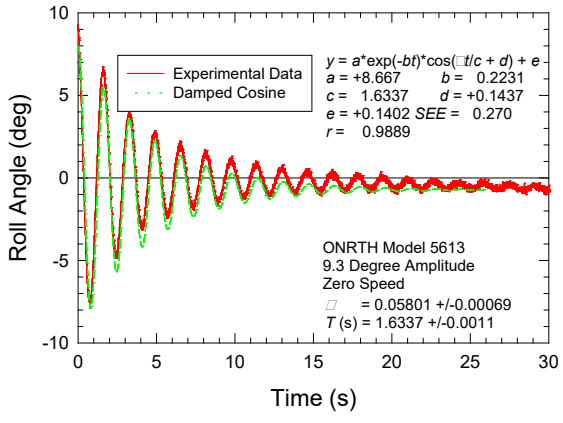

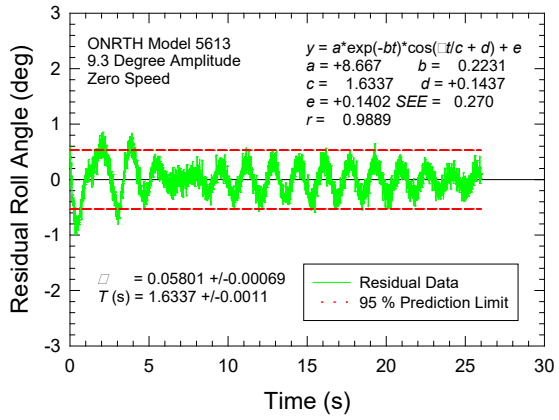

Figure 11: Time series of (a) roll angle and (b) residual at 9.3° with all experimental data.

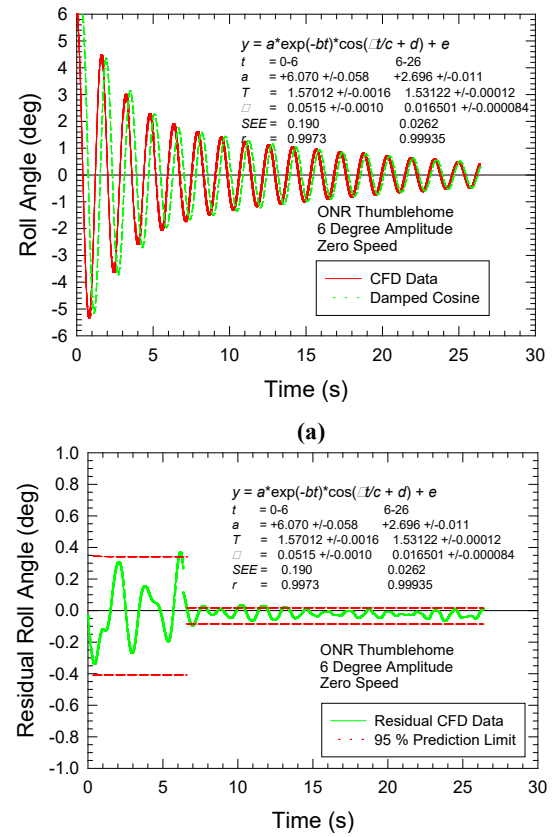

Figure 12: Time series of (a) roll angle and (b) residual at 6° for split CFD data.

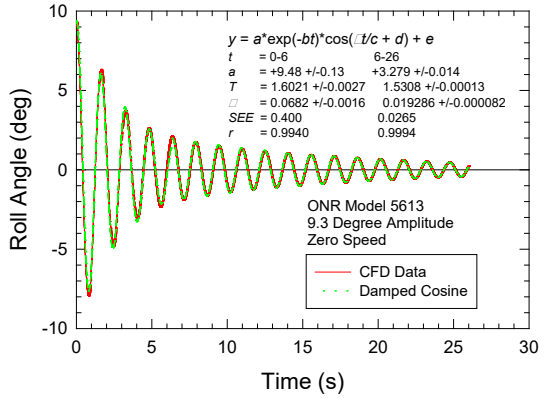

(a)

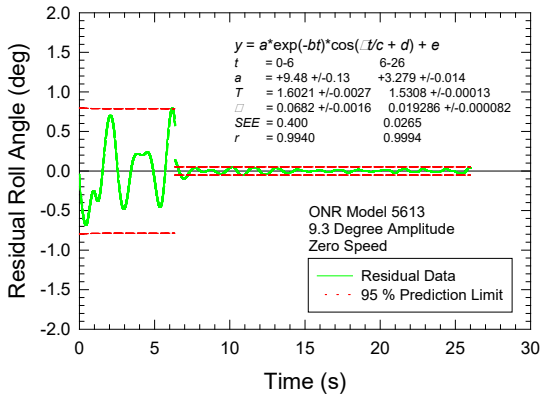

(b)

Figure 13: Time series of (a) roll angle and (b) residual at 9.3° for split CFD data.

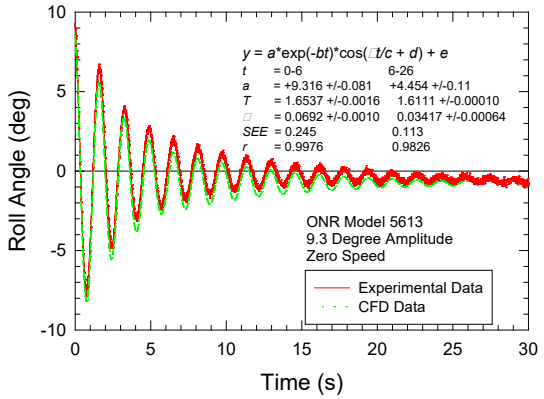

(a)

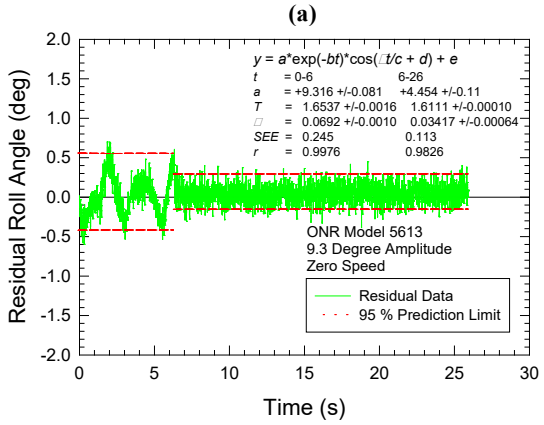

(b)

Figure 14: Time series of (a) roll angle and (b) residual at 9.3° for split experimental data.

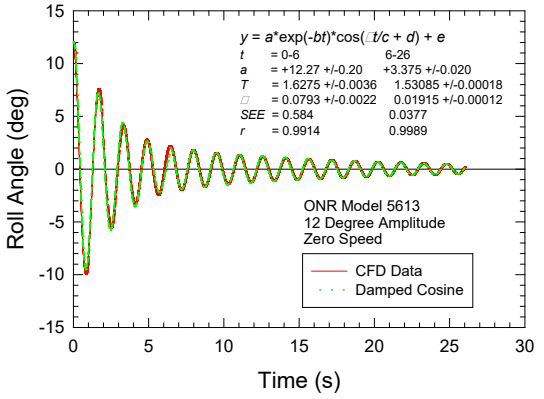

(a)

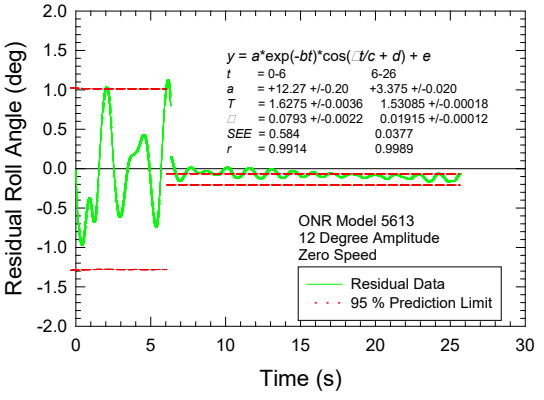

(b)

Figure 15: Time series of (a) roll angle and (b) residual at 12° for split CFD data..

Table 6: Comparison of curve-fit amplitude with the initial from experiment and CFD.

Source	*a* (deg)	26 s	6 s
CFD	6.0	5.066 ±0.059	6.070 ±0.058
CFD	9.3	8.311 ±0.70	9.48 ±0.13
EFD	9.3	8.667 ±0.073	9.316 ±0.081
CFD	12.0	11.36 ±0.18	12.27 ±0.20

The results from curve fit for the exponential cosine function are summarized in Figure 16 and 17 for the roll period and decay coefficient, respectively. For all data and the first 6 s, both the decay coefficient and period increase linearly for the CFD data. The experimental data are outliers relative to the CFD data. For the data after 6 s, both the period and decay coefficient are nealy constant and signficantly less than the results for all data and the first 6 s. The trends are similar to those of Park *et al*. (2009, 2016, and 2017) and may be related to geometric nonlinearity manifested in the backbone curve in Figure 7.

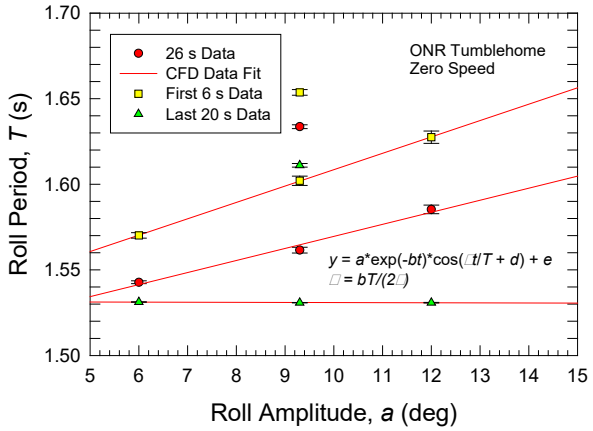

Figure 16: ONRTH roll period from exponential cosine function

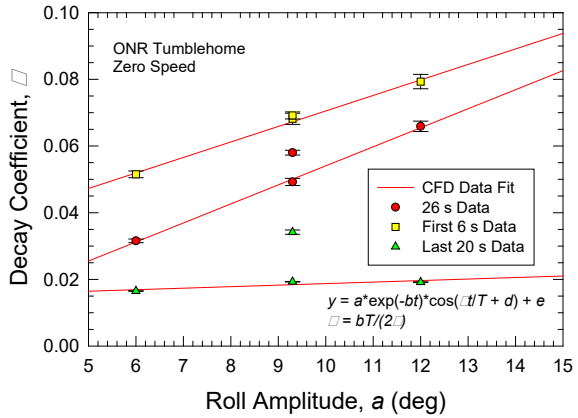

Figure 17: ONRTH roll decay coefficient from exponential cosine function

5. SUMMARY AND CONCLUSIONS

Results for Model 5613, 1/49 scale of the ONR Tumblehome were produced by a URANS simulation for roll decay at three amplitudes, 6.0°, 9.3°, and 12.0°. The CFD were compared to model experiments at 9.3° roll amplitude. The roll decay coefficient was then computed from the data by two methods: exponential cosine function from Equation (22), with nonlinear regression and log-decrement from Equation (1) with linear regression.

Basic formulae for contstrunction of both statistical and prediction intervals were reveiwed for log decrement method. No such review is yet avialable for exponential cosine function fit — commerical software was used for this fit.

Regression with log decrement method was supplemented with analysis of influential observations with Cook's distances. As it could be expected, large peaks were found to be influential, most probably due to nonlinearity of the backbone curve (geometric nonlinearity).

The other manifestation of the geometric nonlinearity was observed with exponential cosine fit. The best fit was observed when the data were divided in two time series, corresponding to large and small values of roll peaks.

This study indicates the dominating influence of nonlinearity on ONR Tumblehome response, which is in contrast to conventional hull behavior such as SIO Melvile (Park *et al*. 2016, 2017), where a single curve fit yields the same decay coefficient as the averaged log-decrement result.

The paper focused on uncertainty quantification of roll decay data. One of the motivations is further propagation of this uncertainty through a dynamical system in order to quantify the uncertainty of the motion response in waves.

The original idea seem to be very simple — uncertainty manifests itself as a randomness. Thus, roll decay coefficients are variables with properties known from the uncertainty analysis. Then, the dynamical system can be considered as a deterministic function of random variables, leading to a distribution of the response. However, more detail consideration produced more questions than answers.

Theis study has raised some questions; what interval should be used for propagation of uncertainty: confidence or prediction? Is the polynomial model for roll damping right when the backbone curve has significant nonlinearity? How to characterize modeling uncertainty? These questions are, indeed, objectives of the future work.

6. ACKNOWLEDGEMENTS

The described effort was partially supported by the US Office of Naval Research under the supervision of Dr. Woei-Min Lin. Uncertainty and outlier calculations for the log decrement method were carried by Dr. Vadim Belenky of NSWCCD.

7. REFERENCES

BIPM, 2008, "Evaluation of measurement data - Guide to the expression of uncertainty in measurement," JCGM 100:2008 GUM 1995 with minor corrections, Joint Committee for Guides in Metrology (JCGM), Bureau International de Poids Measures (BIPM), Sévres, France.

Bishop, R. C., Belknap, W., Turner, C., Simon, B., and

Kim, J. H., 2005 Parametric Investigation on the Influence of GM, Roll Damping, and Above-Water Form on the Roll Response of Model 5613, Carderock Division, Naval Surface Warfare Center Report NSWCCD-50-TR-2005/027, West Bethesda, Maryland, USA

Bulian, G., 2004, "Estimation of nonlinear roll decay parameters using an analytical approximate solution of the decay time history", International Shipbuilding Progress, Vol.51, No. 1, , pp. 5-32.

Dunwoody A.B., 1989, "Roll of a Ship in Astern Seas – Response to GM Fluctuations", *Journal of Ship Research* 33(4), pp. 284-290.

IMO 2006, "MSC.1/Circ.1200 - Interim Guidelines for Alternative Assessment of the Weather Criterion", 24 May.

IMO SDC 8/WP.4/Add.2 Development of Explanatory Notes to the Interim Guidelines on Second generation intact stability criteria. Report of the Drafting Group. London, January 2022.

ITTC, 2021, "Estimation of Roll Damping," 29th International Towing Tank Conference, ITTC Recommend Procedure. 7.5.-02-07-04.5, Rev. 01.

Kawahara, Y., Maekawa, K., and Ikeda Y., 2009, "A Simple Prediction Formula of Roll Damping of Conventional Cargo Ships on the Basis of Ikeda's Method and Its Limitation", Proceedings of the 10th International Conference on Stability of Ships and Ocean Vehicles, (STAB2009), St. Petersburg, Russia, pp. 387-398.

Levine, M. D., Edwards, S. J., Howard, D., Sapsis, T., Weems, K., Pipiras, V., and Belenky, V., 2022 "Data-Adaptive Autonomous Seakeeping" Proc. 34th Symp. Naval Hydrodynamics, Washington, D.C., USA.

Lloyd, A. R. J. M., 1998, Seakeeping: Ship behavior in rough weather, A. R. J. M. Lloyd, Gosport, Hampshire, UK, pp. 364-365.

Myklestad, N. O., 1956, Fundamentals of Vibration Analysis, McGraw-Hill Book Company, New York, pp. 70-76.

Park, Joel T., Hayden, David D., Klamo, Joseph T., and Bishop, Richard C., 2009, Analysis Methodology of Roll Decay Data for Free-Running and Captive Surface Ship Models," Proceedings of the 16th International Conference on Ship and Shipping Research (NAV 2009), Messina, Italy.

Park, J. T., Turner, Charles R., and Melendez, Mark P., 2016, "Physical Properties and Roll Decay with Uncertainty Estimates for DTMB Model 5720, 23rd Scale R/V Melville," Technical Report NSWCCD-50-TR-2016/018, Naval Surface Warfare Center Carderock Division, West Bethesda, MD 20815-5700 USA.

Park, Joel T., Turner, Charles R., and Melendez, Mark P., 2017, "New Methodology in Analysis of Physical Properties and Roll Decay with Uncertainty Estimates for Surface-Ship Model Experiments," 30th American Towing Tank Conference, Naval Surface Warfare Center Carderock Division, West Bethesda, MD USA, Paper ATTC2017-0020.

Pipiras, V., Howard, D., Belenky, V., Weems, K., and Sapsis T. 2022, "Multi-Fidelity Uncertainty Quantification and Reduced-Order Modeling for Extreme Ship Motions and Loads" Proc. 34th Symp. Naval Hydrodynamics, Washington, D.C., USA.

Weems K. and Sapsis T., 2022 "Recent Development with Reduce Order Models (ROM)" Proc. of 18th ISSW, Gdansk, Poland.